Lowland Technology International 2020; Volume 22(2): 249-257
International Association of Lowland Technology (IALT): ISSN 1344-9656

Research Paper

Ground penetrating radar attributes analysis for detecting underground artificial structures in urban areas, Vietnam

C.V.A. Le [1] and T.V. Nguyen [2]

ARTICLE INFORMATION

Article history:

Received: 24 July, 2019
Received in revised form: 6 June, 2020
Accepted: 12 June, 2020
Publish on: 06 September, 2020

Keywords:

Ground penetrating radar
Reflection wave
Migration
Energy

ABSTRACT

Maps of underground construction works for maintenance, building and planning tasks are essential in urban areas. Ground penetrating radar (GPR) has shown effectiveness by providing high-resolution imaging of subsurface structure. Reflection/ diffraction from boundaries, singular objects, or edges of anomalies could lead to meaningful events like strong signals or shapes of hyperbolae in the common offset unmigrated GPR sections. In urban areas, although the shielded antennas help the GPR machine to remove most of man-made noises transmitted from the air, the GPR data are still heavily contaminated by types of noises. Concerned objects (i.e., underground pipes, tunnels, and subsurface structures) can be effectively revealed by applying the GPR attributes that are calculated from the processed abundant GPR data information as enhancement of ratio between signal over noise. In our paper, for the GPR data surveyed in Ho Chi Minh City, Ba Ria – Vung Tau Province, and Dong Nai Province, Vietnam, we have utilised a set of GPR attributes (i.e., amplitude before/after migration, cosine-of-instantaneous phase, and energy) and volume rendering (i) to define 2D/3D anomalies relating to underground manmade system, and (ii) to uncover hidden underground objects with illumination of upper concrete construction steel net of buildings.

1. Introduction

The application of Ground Penetrating Radar (GPR) is widely recognised nowadays when many GPR projects are conducted in many areas from civil engineering, groundwater prospecting, mineral exploration, environmental geophysics, archaeology to geology investigations (Ercoli et al., 2014; Lai et al., 2018; Liner and Liner, 1997; Nguyen et al., 2017; Nguyen et al., 2010; Nguyen et al., 2005; Rashed and Al-Garni, 2013; Zhao et al., 2015b; Zhao et al., 2016). The principle of the GPR method is to emit high-frequency pulses down to the subsurface environment and reflected waves are received to reveal characteristics of the earth environment. The investigated depth is quite shallow, ranging from meters to tens of meters depending on the conductivity/ impedance of environment layers and frequency. Impedance contrast between an underground anomaly and surrounding environment ignites reflection/ diffraction events in the GPR traveltime section. This emphasises GPR practical to the investigation of underground artificial structures.

Effectiveness of seismic attributes (Chopra and Marfurt, 2007; Le et al., 2016; Zhao et al., 2015a) which are extracted from conventionally processed seismic data can motivate interpreters working with GPR to apply their ideas into GPR areas. Many research papers are used to understand subsurface structures. For examples, Zhao et al. (2016) have applied texture attributes for GPR signals to express remnants of the Bronze Age and geology structures. Sinkholes in old mining alert human awareness of safety can be detected by using GPR attributes (Tomecka-Suchoń and Marcak, 2015).

For civil engineering, infrastructure planning and development in urban zones, map of underground objects (i.e., electric pipes systems and tunnel) is

[1] Lecturer, Department of Geophysics, Faculty of Physics and Engineering Physics, University of Science, Vietnam National University Ho Chi Minh City, VIETNAM, lvacuong@hcmus.edu.vn. Corresponding author.
[2] Lecturer, Department of Geophysics, Faculty of Physics and Engineering Physics, University of Science, Vietnam National University Ho Chi Minh City, VIETNAM, nvthuan@hcmus.edu.vn
Note: Discussion on this paper is open until March 2021

essential. Underground pipes are located with conventionally processed GPR data in Ho Chi Minh City, Vietnam (Nguyen et al., 2017). Besides, the existence of steel mesh is often to help to cover or protect some more important structures below it (Voigt et al., 2004). Especially, steel mesh in concrete can be revealed with the equal-distance structure in GPR image (Liu et al., 2007; Sangoju and Ramanjaneyulu, 2015).

2D/3D visualisation for GPR data can illustrate underground anomalies effectively. 3D GPR analysis can image shallow subsurface geology structures (i.e., faults, Central Appennines, Italy (Ercoli et al., 2014) and bryozoan limestone (Sigurdsson and Overgaard, 1998)).

Conventional workflow for processing GPR is to convert GPR raw data with weak amplitudes and noisy appearances into interpretable processed GPR data. However, the processed GPR data could not provide all visible underground objects by its conventional amplitude (Boeniger and Tronicke, 2010). Therefore, GPR attributes are applied to add a different aspect to interpret the processed GPR (Park et al., 2018; Zhao et al., 2016). Note that GPR attributes just extract some meaningful information/characteristics from the GPR abundant data information.

We give credit to Common Offset (CO) GPR data for recognition of diffractors through their hyperbola curves. Using migration to collapse diffracted curves, the processed GPR just give correct positions of the geology structures (i.e., layer, fault, cave, sinkhole) and diffractors (i.e., pipes, tunnel, steel mesh net); however, we are easily confused by the strong amplitudes of the diffractors with other random strong-amplitude noises. That inspires us to combine both CO data and migrated data or different GPR attributes at the same time to interpret the data and to figure valuable events. For example, each meaningful diffractor has the hyperbola shape in conventionally CO format and also has strong energy after migration. Representation of the overlay image, including its hyperbola and strong energy, can confirm the location of the diffractor.

In our research, different GPR attributes consisting of GPR amplitude, instantaneous attribute as phase, and energy of its migrated amplitude are applied to process and analysis GPR data measured in rural zones, Vietnam. We also utilise 3D visualisation to image the underground anomalies and reveal some hidden structures that are difficultly seen in the conventional GPR data.

2. Methodology

GPR data measurement in our research follows Common Offset style where distance of transmitter and receiver antennas is fixed. The equipment is Detector Duo IDS machine made by Italy (**Fig. 1**). For detecting the existence of underground manmade constructions (i.e., pipelines, water pipe), we often have set up 2D profiles across / parallel to the potential direction of the pipes. The intersection point of the 2D across profiles

Fig. 1. A GPR machine survey, IDS Detect Duo, Italy

and the pipe direction plays a role as a diffractor and represents a hyperbola in the GPR section (Nguyen et al., 2017; Prego et al., 2017). This useful characteristic helps interpreters to define the pipeline.

For interpreting the GPR data, there are two processes discussed: (i) the conventional workflow to transform the raw measured data into the processed data in which interpretation work can be started, and (ii) the work of calculating GPR attributes for further interpretation with the input data as the processed data made in the process (i). All the GPR attributes and the processed data of the process (i) are put in the professional software, OpendTect (dGB Earth Sciences, 2015) for defining underground anomalies.

2.1 Conventional workflow

During wave propagation, the electromagnetic energy dissipates, is absorbed and noise-contaminated by surrounding environment before arriving at the receiver antenna. The conventional workflow is to compensate its loss energy and to remove the noise (i.e., background noise, 1DC noise, and high/ low frequency noises) (Fisher et al., 1996; Nguyen et al., 2017; Park et al., 2018; Rashed and Al-Garni, 2013). The conventional workflow consists of some processing steps (Fisher et al., 1996; Nguyen et al., 2017). Our raw data are processed through: (i) Move-start time, (ii) subtract DC shift, (iii) background removal, (iv) subtract mean (dewow), (v) gain function, (vi) time-cut, and (vii) bandpass butterworth. In the whole paper, the term, CO data, means that the raw GPR data has been applied with the seven steps. Finally, we applied Kirchhoff migration to the CO data. Migration velocities were chosen by analysing diffraction curves, leading to average value as 0.1m/ns.

3.3 GPR attributes

GPR attributes share the same idea with seismic attributes when the GPR attributes just take each side of characteristics of abundant-information GPR signal depending all the purposes of each GPR attribute.

Hilbert transformation considers GPR waveform as complex signal for separating each GPR wavelet into two distinct parts, real and imaginary (Chopra and Marfurt, 2007; dGB Earth Sciences, 2015; Park et al., 2018). The real part is allocated to the absolute amplitude of one wavelet while imaginary one reflects its phase. The imaginary part, instantaneous phase (Chopra and Marfurt, 2007), is used for expressing continuity and discontinuity of events. Theoretically, the parameter should be similar along a horizon and vary if the layer changes laterally. Cosine of instantaneous phase (Chopra and Marfurt, 2007; Subrahmanyam and Rao, 2008) (so-called cosine-of-phase in our research) could also enhance the continuity of events (i.e., layer or diffraction curve) but be smoother than phase.

Energy measure is square of each GPR amplitude through a window gate (dGB Earth Sciences, 2015). This parameter is a good indicator for reflection events if energy variation exists in the reflector (Boeniger and Tronicke, 2010).

3.4 Image overlay

We applied the idea that overlay image (Le et al., 2016) of different attributes could be useful in locating a meaningful anomaly. Existence of a pipeline could lead to a hyperbola in GPR section and a strong amplitude focus after migration (Nguyen et al., 2017). The migrated GPR section can include many strong amplitudes that could be misunderstood as noise or signal. Therefore, coupling strong energy point (after migration) with its hyperbola shape (before migration) can be of highly usefulness to define the existence of a meaningful anomaly (**Fig. 2**). The hyperbola shape could be achieved from the cosine-of-instantaneous phase attribute. The overlaid amplitude could be energy measure of migrated data.

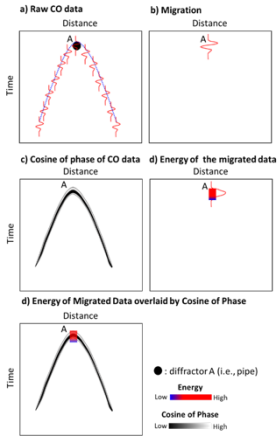

Fig. 3. Schematic of the overlay image of two different attributes to express a diffractor: Energy of the migrated data and the cosine-of-phase. a) Raw CO data expressing a hyperbola resulted by the diffractor A. b) Migration is applied to raw CO data for converging the hyperbola into one high singular wavelet as known as the diffractor A. c) The cosine-of-phase attribute for highlighting the continuity of the hyperbola in the CO data. d) Energy of the migrated data (Fig. 2b) are expressed in two oscillation and color representations. d) Overlay image by energy of migrated data and the cosine-of-phase for specifying existence of the diffractor

3. Results

We have analysed three GPR datasets for locating underground objects. The objects are water tunnel, a bunch of electric pipes, and a septic tank covered by a steel mesh. For all these data, our purpose is to use GPR attributes to delineate the underground effectively. The datasets are using Detect Duo IDS machine, Italy. Its measurement style follows CO tradition. The frequency data used for interpretation is 700 MHz. Our attributes results are compared with the prior information provided by industrial/commercial companies or seen in the field trip.

3.1 Data 1: Phu Nhuan District, Ho Chi Minh City, Vietnam

In the data, we have tried to investigate underground anomalies (i.e., electric pipes, drainage water pipe) in Nguyen Kiem Street, Phu Nhuan District, Ho Chi Minh City (**Fig. 3**). There are six 2D GPR profiles, including three in-lines and three crosslines. The whole interest area is around 12-meter square. To understand this geophysical dataset, we have done two processes: (i) data analysis by using the conventional workflow and the GPR attribute calculation (cosine-of-phase and energy) mentioned in the **Methodology** section, and (ii) putting all the GPR processed data into the 3D volume for further interpretation.

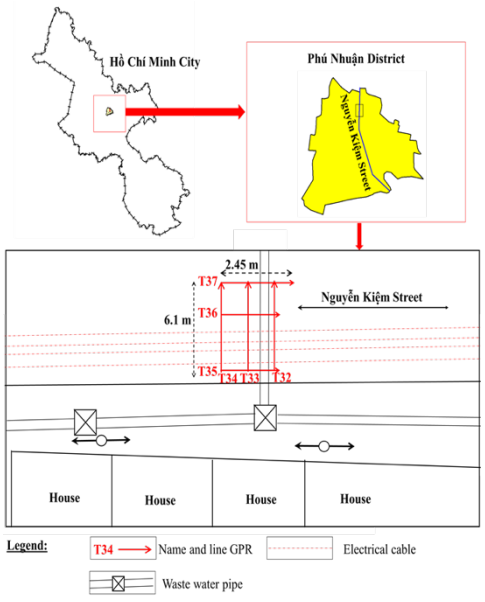

Fig. 2. Survey setting map for detecting underground anomalies in Nguyen Khiem Street, Phu Nhuan District, Ho Chi Minh City, Vietnam

We have dealt with the workflow for transforming the raw data into the processed data that can be interpreted. The conventional workflow includes move-start-time, filtering (i.e., removing background noise, dewow, bandpass filtering), amplitude gaining, and migration (see **Fig. 4b**).

For interpretation, the processed data can be of effective use for revealing meaningful signals connecting underground anomalies in OpendTect. We have interpreted two kinds of underground: (i) strong amplitudes (**Fig. 4**); and (ii) weak but continuous signals in the deeper depth (**Fig. 5**).

(i) Strong amplitudes: There are quite strong hyperbolae in the three profiles T32, T33, and T34 at the specified time 12 ns (see cyan arrows in **Fig. 4a**). One prolonged anomaly line can be explained by these hyperbolae and a layer of strong amplitudes in the other profile T35 at top time around 12ns (**Fig. 4**). The anomaly line as the strong amplitudes is visualised in all the images of CO data, migrated, energy data. It is interpreted as a bunch of electric wires shown in the **Fig. 3**. (the dashed red line). We have used volume render to image the 3D pink prolong anomaly (see cyan arrow in **Fig. 4d**). Its top depth is around 0.6m with the migrated velocity 0.1m/ns.

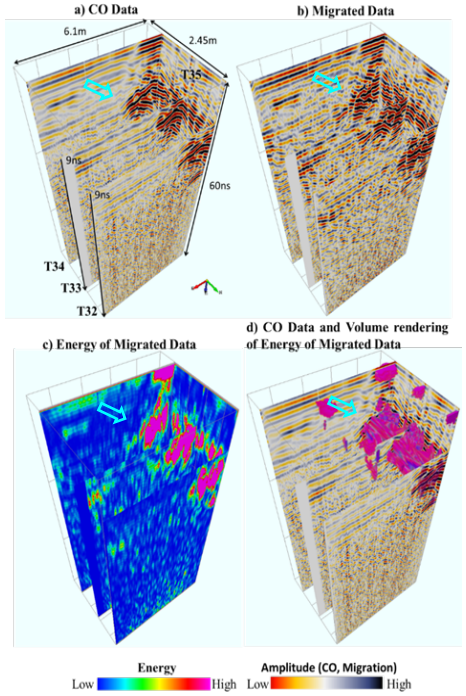

Fig. 4. Representation of different attributes for imaging electric wires. Strong amplitudes in CO data (a), migrated data (b), energy of migrated data (c) and the 3D bulk line express the electric wires (see cyan arrows)

(ii) Weak amplitudes: the weak amplitudes are hardly seen as meaningful signal in the CO data section (**Fig. 5a**) by naked eyes. We have applied different attributes for illuminating these weak amplitudes reflecting a signal if existence. After using migration and computing the energy attribute for the migrated data, we can detect some strong values at the time around 18ns-20ns in the energy section (see white arrows in **Fig. 5c** and **Fig. 5d**). Overlay image of the energy with the cosine-of-phase could provide a better representation of one new anomaly. Peaks of the three curves of cosine-of-phase seen in the bigger time (18ns-20ns) are compatible with the strong energy values (see white arrows in **Fig. 5d**). It leads to the interesting interpretation that the new event extracted from the attributes of weak signals is interpreted as a drainage water pipe (see the wastewater pipe in **Fig. 3** and the white dashed ellipse in **Fig. 5**). The exposed footprint of the drainage water pipe is drawn in **Fig. 3** and **Fig. 5**. Its depth is around 0.9m with the migrated velocity 0.1m/ns.

Strong amplitudes in such attributes as CO data, migrated, and energy sections can provide the place where reflection/ diffraction occurs while cosine-of-instantaneous phase can estimate continuity of boundary or diffraction curves of an anomaly. The strong amplitudes could show the existence of bunches of electric wire while the cosine-of-phase could show the curves of the water pipe in the light of strong energy values. Therefore, their combination could enhance the interpretation. The existence of electric wires and the drainage water pipe are the prior information (see **Fig. 3**) provided by the Dai Viet Investment and Development Water Environment Joint, Vietnam (Dai Viet Company).

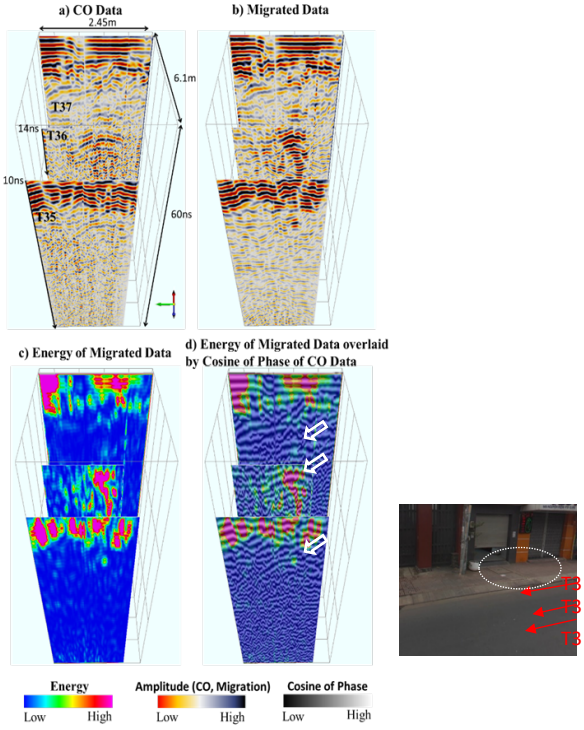

Fig. 5. Representation of different attributes for detecting drainage water pipe. The overlaid image of two attributes (d) could enhance its existence through strong energy of migrated data and the cosine-of-phase curve (see white arrows). The footprint of the drainage water pipe (Google Maps, 2019) is shown by the white dashed ellipse

3.2 Data 2: Tan Thanh District, Ba Ria – Vung Tau Province, Vietnam

For maintenance purpose, location of supplying water tunnel needs to be defined in an area, Tan Thanh District, Ba-Ria – Vung Tau Province, Vietnam. According to prior information of Hai Lan Survey Construction Consultancy Company Limited (Hai Lan Company) and the Vietnam Urban and Industrial Zone Development Investment Corporation (IDICO), we have known that there is a water pipe in the pavement of the NB1 street (see black – blue line in **Fig. 6**).

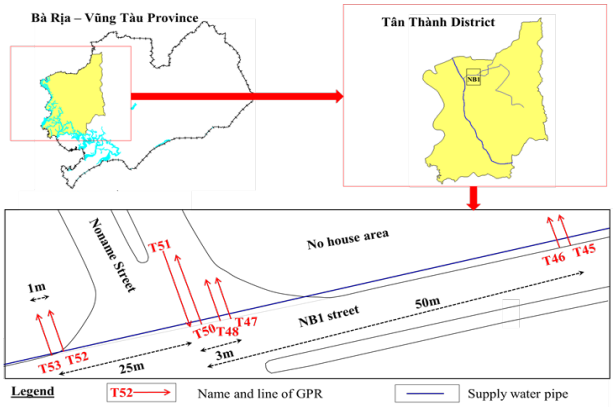

Fig. 7. Survey setting map for detecting underground water tunnel in Tan Thanh District, Ba Ria – Vung Tau Province

We have processed eight 2D GPR profiles with their length around 6.5m. The raw data are processed into interpretable CO data, migrated, cosine-of-phase, and energy sections (see **Fig. 7** and **Fig. 8**) to answer the location of the underground water pipe.

In **Fig. 7**, near the origin O, there are three visible hyperbolae with specified time ranges from 10ns to 15 ns (depth ranging from 0.5 to 0.75m with the migrated velocity 0.1m/ns) (see the CO data in profiles T53, T46, and T45) expressing one extended anomalous line that could be interpreted as water supplying tunnel (see white arrows in **Fig. 6**). For the overlaid images between energy and cosine-of-phase attributes, the extended anomalous line is confirmed by the strong energy amplitudes and the hyperbola curves of cosine-of-phase. In the profile T52 (**Fig. 7**), although we do not see its hyperbola appearance, there is still a strong energy point in the energy and overlaid images following the direction of the interpretable water tunnel.

Defining the position of the water tunnel in the Noname street, some incomplete diffracted curves (see T50 and T51) are still considered (**Fig. 8**). Hyperbolae are not fully captured in all the profiles T47, T48, T50, and T51 (**Fig. 8**). Interestingly, a layer of many small hyperbolae with equal distance in the time around 5ns locates upper positions of the incomplete curves or strong energy (see cyan arrows in the overlaid images of the four profiles (**Fig. 8**)). This gives us the idea that the layer interpreted as steel net is used for protecting the more important object below. Note that a water pipe locating in the street without any protection (i.e., strong cover) is vulnerable because of the pressure of heavy transportation.

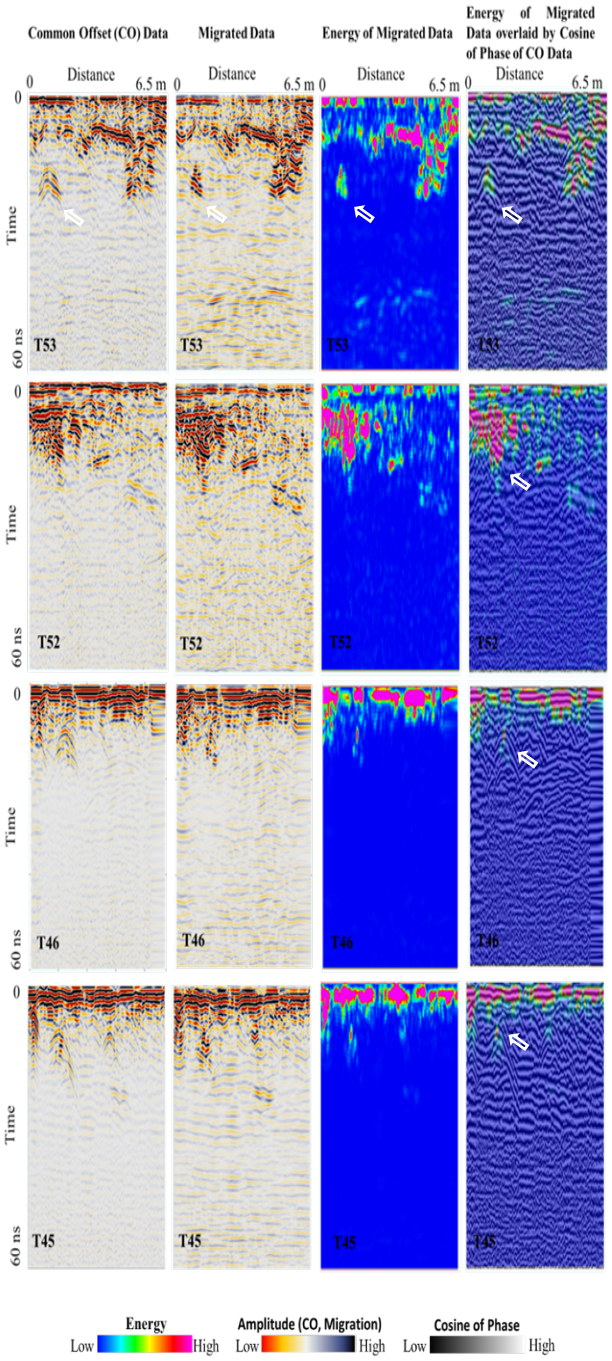

Fig. 6. The 2D GPR profiles of different attributes for revealing existence of the water supplying tunnel, Ba Ria – Vung Tau Province. Most the overlaid images of the attributes define the water supplying target except the profile T52 (see white arrows). Note that the energy section of the profile T52 also defines a meaningful event that could be interpreted as the water supplying one

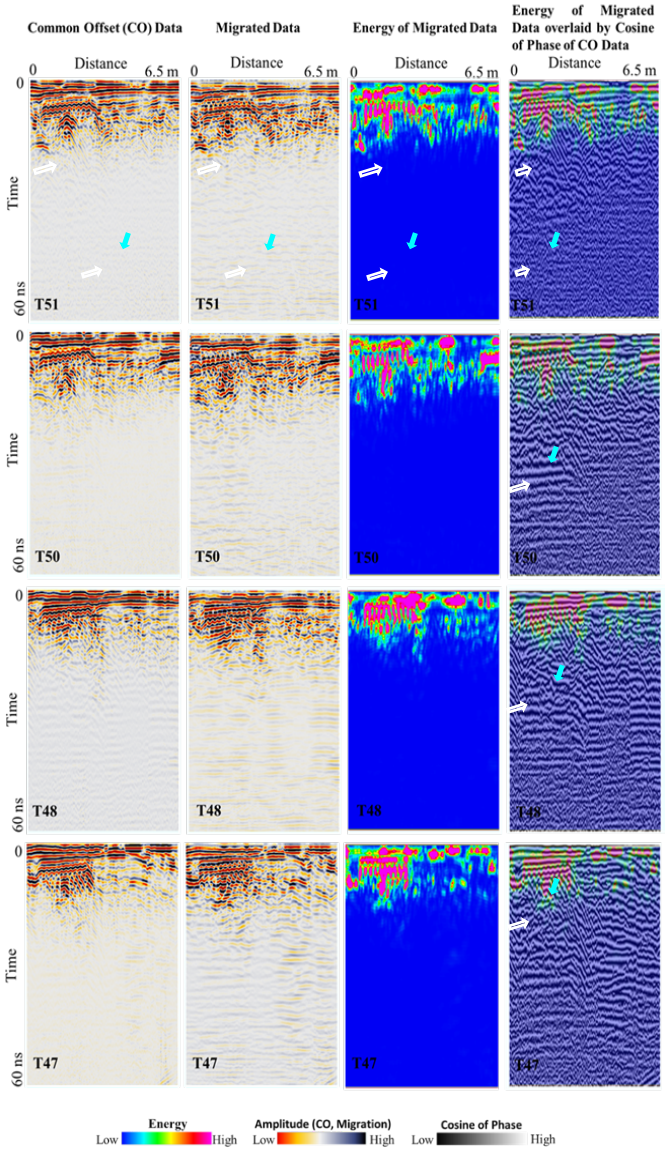

Fig. 8. The 2D GPR profiles of different attributes for revealing existence of the steel mesh (see cyan arrows) and the supplying water tunnel (see white arrows), Ba Ria – Vung Tau Province

After viewing the interpretable steel net as the good indicator for a potential deeper anomaly, we focused on its below zone in four overlaid images (**Fig. 8**) to see the meaningful signal of the water tunnel. The cosine-of-phase attribute (see the overlay image in **Fig. 8**) can enhance the hyperbola curve stemming from a diffraction object and the high energy attribute show the precise location of the diffraction helping to differentiate the water tunnel (diffractor) rather than other strong reflection boundary structures. 3D visualisation of the underground water tunnel (see white arrow in **Fig. 9**) and the steel net (see cyan arrows in **Fig. 9**) can be displayed by the energy of GPR migrated amplitude.

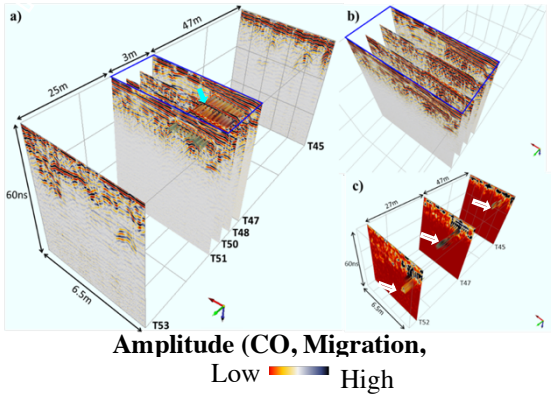

Fig. 9. 3D visualization for revealing the steel net (see cyan arrow in Fig. 9a) and the water supplying tunnel (see white arrows in Fig. 9c) in Ba Ria – Vung Tau Province. b) The CO data profiles are shown without the 3D steel net. c) The sections of energy of the migrated data are coupled with the 3D water supplying tunnel.

3.3 Data 3: Daemyung Company, Dong Nai Province

The purpose of our survey in the Daemyung company, Dong Nai Province is to define the location of septic tank in its canteen zone (see the red rectangular zone in **Fig. 10**). The GPR survey is illustrated in **Fig. 10**. We have set up three inline and crossline GPR profiles (T1, T2, and T3) to image the septic tank area. The conventionally processed GPR data and their attributes are computed following the procedure in the **Methodology** section.

In **Fig. 11**, the steel net is visible in the three overlaid sections (see the white dashed rectangles). Steel net appears as many strong-amplitude points in the migrated data. The steel net layer being formed by the strong energy zones of migrated data and by peaks of small white hyperbolae in the cosine-of-phase sections increases our awareness about the existence of an underground anomaly below. This anomaly is interpreted as the zone of the septic tank suitable with the prior information of the Daemyung Company.

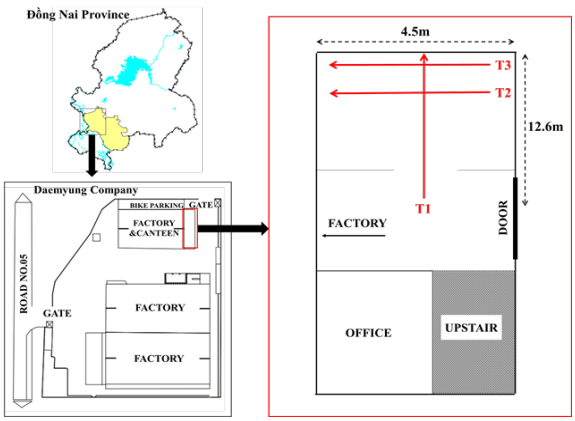

Fig. 10. Survey setting map for detecting an underground septic tank in a canteen of Daemyung Company, Dong Nai Province

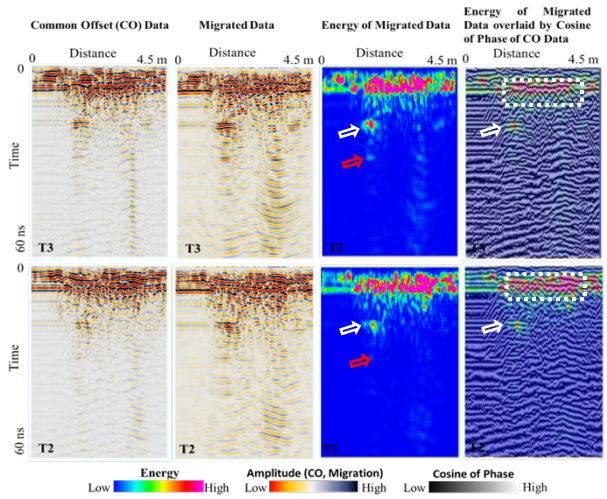

Fig. 11. The 2D GPR profiles (T2 and T3) of different attributes for revealing existence of the steel mesh, Dong Nai Province (see white dashed rectangular). A strong reflection is interpreted as boundary between the septic tank with the surrounding environment (see white arrow) and other reflection with smaller energy is interpreted as the multiple noise of the boundary (see red arrow)

Below the steel net, we can see strong reflection as a layer (see white arrow) and one more reverberation (see red arrow) of the layer (see **Fig. 11**, **Fig. 12**, and **Fig. 13**). We think that the layer (the white arrow) may be bottom of the tank. Importantly, the area of the tank can be observed in the GPR sections as our answer to the survey purpose. 3D visualisation of the interpretable septic tank is shown with the 3D GPR representation (**Fig. 13**).

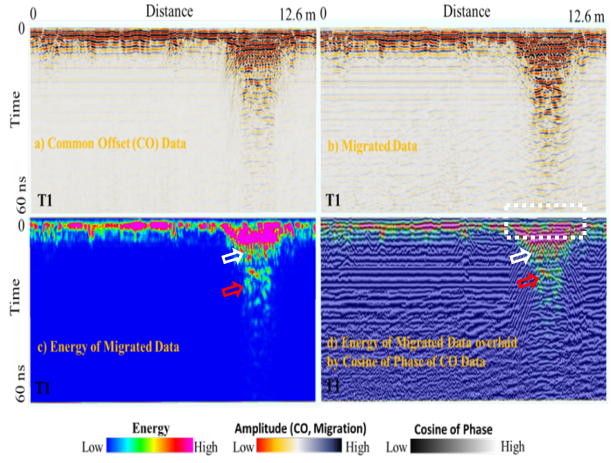

Fig. 12. The 2D GPR profile (T1) of different attributes for revealing existence of the steel mesh, Dong Nai Province (see white dashed rectangular). A strong reflection is interpreted as boundary between the septic tank with the surrounding environment (see white arrow) and other reflection with smaller energy is interpreted as the multiple noise of the boundary (see red arrow)

4. Conclusion

GPR data can provide an excellent tool for examining underground anomalies while GPR attributes can deliver a good insight of the images. We have applied different GPR attributes plus raw and processed data for the distinct urban areas in southern Vietnam. For all the three cases, the underground objects as electric pipes, water tunnel and underground septic tank can be well-defined. Importantly, GPR attributes and the overlay image of cosine-of-phase and energy attributes could be of great cooperation to explore useful underground anomalies. Their 3D visualisation through setting the 2D GPR profiles can enhance images of the anomalies. While strong amplitudes of a GPR attribute could express their existences through reflection/diffraction, cosine-of-phase sections can help an interpreter to follow the continuity of their reflection/ diffraction curves. Existence of steel net is good indicator for the interpreter to search for more useful information of any other anomaly below its location.

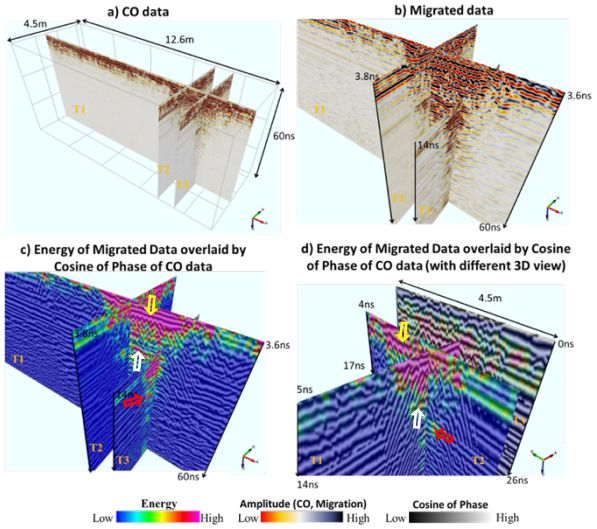

Fig. 13. 3D visualization for revealing the zone of the steel net and the septic tank in Dong Nai Province. Existence of the steel net (see yellow arrows) can be an indicator to an important object (known as the septic tank in this data). The boundary between the septic tank and the surrounding environment is shown via the strong reflection (see white arrows). Its reflection multiple noise is seen as red arrows

Acknowledgements

This research is funded by Vietnam National University HoChiMinh City (VNU-HCM) under grant number C2019-18-08. We would like to give our thanks to Dr. Thong Kieu for his useful advice. Our special thanks go to Mr. Vu Lam for his language revision. We are also thankful to the companies as Dai Viet Company, Hai Lan Company, IDICO Corporation, and Daemyung Company, who provide us with prior information during our survey. We are also grateful to dGB Earth Sciences and Curtin University for providing access to software tools

References

Boeniger, Urs, and Jens Tronicke., 2010. Improving the interpretability of 3D GPR data using target–specific attributes: application to tomb detection. Journal of Archaeological Science, **37** (2):360-367.

Chopra, Satinder, and Kurt J. Marfurt., 2007. Seismic attributes for prospect identification and reservoir characteriztion. Edited by Stephen J. Hill, SEG Geophysical Development Series No. 11. United States of America: Tulsa, Okla. (8801 South Yale St., Tulsa OK 74137-3175): Society of Exploration Geophysicists

dGB Earth Sciences. OpendTect dGB Plugins User Documentation version 4.6, http://opendtect.org/relman/4.6.0/unpacked/4.6.0/doc/User/dgb/chapter2.3_attributes_with_steering.htm.

Ercoli, Maurizio, Cristina Pauselli, Alessandro Frigeri, Emanuele Forte, and Costanzo Federico., 2014. 3-D GPR data analysis for high-resolution imaging of shallow subsurface faults: the Mt Vettore case study (Central Apennines, Italy). Geophysical Journal International, **198** (1):609-621.

Fisher, Steven C, Robert R Stewart, and Harry M Jol. 1996. Ground penetrating radar (GPR) data enhancement using seismic techniques. Journal of environmental and engineering geophysics, **1** (2):89-96.

Google Maps, 2019. An image of Nguyen Kiem Street, Phu Nhuan District, Ho Chi Minh City, Vietnam.

Lai, Wallace Wai-Lok, Xavier Derobert, and Peter Annan., 2018. A review of Ground Penetrating Radar application in civil engineering: A 30-year journey from Locating and Testing to Imaging and Diagnosis. NDT & E International 96:58-78.

Le, Cuong V. A., Brett D. Harris, Andrew M. Pethick, Eric M. Takam Takougang, and Brendan Howe., 2016. Semiautomatic and Automatic Cooperative Inversion of Seismic and Magnetotelluric Data. Surveys in Geophysics **37** (5):845-96. doi: 10.1007/s10712-016-9377-z.

Liner, Christopher L., and Jeffrey L. Liner., 1997. Application of GPR to a site investigation involving shallow faults. The Leading Edge, **16** (11):1649-51. doi: 10.1190/1.1437545.

Liu, Lanbo, Kuang He, Xiongyao Xie, and Jun Du., 2007. Image enhancement with wave-equation redatuming: application to GPR data collected at public transportation sites. Journal of Geophysics and Engineering, **4** (2):139.

Nguyen, Thuan V., Cuong V. A. Le, Van T. Nguyen, Trung H. Dang, Triet M. Vo, and Lieu N.L. Vo., 2017. Energy Analysis in Semiautomatic and Automatic Velocity Estimation for Ground Penetrating Radar Data in Urban Areas: Case Study in Ho Chi Minh City, Vietnam. International Conference on Geo-Spatial Technologies and Earth resources, Ha Noi, Vietnam.

Nguyen, Van Giang, Guy Marquis, and Minh Le., 2010. EM and GPR investigations of contaminant spread around the Hoc Mon waste site, Vietnam. Acta Geophysica, **58** (6):1040-1055.

Nguyen, Van Giang, Jerzy Ziętek, Ba Duan Nguyen, Jerzy Karczewski, and Tomisław Gołębiowski., 2005. Study of geological sedimentary structures of Mekong river banks by Ground Penetrating Radar: forecasting avulsion-prone zones. Acta Geophysica Polonica, **53** (2):167-181.

Park, Byeongjin, Jeongguk Kim, Jaesun Lee, Man-Sung Kang, and Yun-Kyu An., 2018. Underground object classification for urban roads using instantaneous phase analysis of ground-penetrating radar (GPR) data. Remote Sensing, **10** (9):1417.

Prego, FJ, M Solla, I Puente, and P Arias., 2017. Efficient GPR data acquisition to detect underground pipes. NDT & E International, 91:22-31.

Rashed, Mohamed A, and Mansour A Al-Garni., 2013. On the application of GPR for locating underground utilities in urban areas. Arabian Journal of Geosciences, **6** (9):3505-11.

Sangoju, Bhaskar, and K Ramanjaneyulu., 2015. Estimation of rebar diameter in concrete structural elements using ground penetrating radar. NDE2015, Hyderabad.

Sigurdsson, Thrainn, and Torben Overgaard., 1998. Application of GPR for 3-D visualization of geological and structural variation in a limestone formation. Journal of Applied Geophysics, **40** (1):29-36.

Subrahmanyam, D., and P.H. Rao., 2008. Seismic Attributes- A Review. 7th International Conference and Exposition on Petroleum Geophysics. Hyderabad2008.

Tomecka-Suchoń, Sylwia, and Henryk Marcak., 2015. Interpretation of ground penetrating radar attributes in identifying the risk of mining subsidence. Archives of Mining Sciences, **60** (2):645-56.

Voigt, Thomas, Van K Bui, and Surendra P Shah., 2004. Drying shrinkage of concrete reinforced with fibers and welded-wire fabric. ACI Materials Journal, **101** (3):233-41.

Zhao, Tao, Vikram Jayaram, Atish Roy, and Kurt J. Marfurt., 2015. A comparison of classification techniques for seismic facies recognition. Interpretation.

Zhao, Wenke, Emanuele Forte, Sara Tiziana Levi, Michele Pipan, and Gang Tian., 2015. Improved high-resolution GPR imaging and characterization of prehistoric archaeological features by means of attribute analysis. Journal of Archaeological Science, **54**:77-85.

Zhao, Wenke, Emanuele Forte, and Michele Pipan., 2016. Texture attribute analysis of GPR data for archaeological prospection. Pure and Applied Geophysics, **173** (8):2737-2751.

Symbols and abbreviations

GPR	Ground penetrating radar		background removal, (iv) subtract mean
CO	Common Offset		(dewow), (v) gain function, (vi) time-cut,
CO data	The raw GPR data is analysed with the		and (vii) bandpass butterworth
	seven processing steps, (i) Move-start	ns	nano second
	time, (ii) subtract DC shift, (iii)	m	meter